Characterization of a high-performance portable GC with a chemiresistor array detector†

Qiongyan Zhong,[a] William H. Steinecker[b] and Edward T. Zellers*[ab]

Received 28th June 2008, Accepted 26th September 2008
First published as an Advance Article on the web 12th November 2008
DOI: 10.1039/b810944c

The laboratory characterization of a novel, second-generation portable gas chromatograph (GC) prototype designed for trace-level determinations of complex mixtures of volatile organic compounds (VOC) is described. The instrument incorporates a small, multi-stage adsorbent preconcentrator/injector (PCI), two series-coupled separation columns with fast, independent temperature-programming capabilities and junction-point pressure/flow control, and a detector consisting of an array of microfabricated chemiresistor (CR) sensors coated with thiolate-monolayer-protected gold nanoparticle films. Response patterns from the CR array are used in conjunction with chromatographic retention times to identify eluting mixture components. Scrubbed ambient air is used as the carrier gas. Enhancements in design relative to a previously reported first-generation prototype instrument have led to significant reductions in limits of detection as well as improvements in resolution, reliability, flexibility, and convenience. Key features of the instrument are characterized, with an emphasis on the tradeoffs in sensor array performance associated with operation at different temperatures and flow rates. The separation of a preconcentrated mixture of 31 VOCs in < 7 minutes is demonstrated. Projected detection limits are in the ppt range for most compounds, assuming a 1 L sample volume.

Introduction

Characterizing the spatial and temporal variations in airborne volatile organic compounds (VOC) concentrations can be critical to the assessment of human exposure levels, emission-source locations and intensities, building ventilation effectiveness, and ambient environmental contaminant distributions. Where speciation of VOC mixture components is required, portable gas chromatographic (GC) instruments offer numerous potential advantages.[1]

On-site VOC monitoring with field-portable GCs has been practised for nearly 30 years[2,3] and numerous manufacturers currently market compact instruments suitable for field deployment.[4–10] Increasingly, conventional approaches to separation and detection have given way to new approaches made possible by advanced technologies. For example, the use of low-thermal-mass column modules with embedded heaters and temperature sensors now permits faster temperature programming of capillary columns at lower power than with conventional ovens.[11,12] A growing number of commercial GCs are incorporating microfabricated components for injection,[7,8] separation,[13,14] and detection[6,8,10] and several reports on prototype micro-GCs have appeared recently.[13–18]

Published reports on portable GC applications are generally limited to determinations of VOC mixtures of < 20 compounds.[19–22] Although this does not represent any sort of fundamental limit on the complexity of mixtures that can be analyzed, it does provide a benchmark. Where single-channel detectors are used, speciation relies on retention times, which are subject to shifts in field settings. Continued progress is being made toward smaller and more rugged portable GC detectors based on mass-[9,23,24] and ion-mobility-[25–27] spectrometries, which provide an added dimension to the analysis that reduces reliance on retention time for qualitative information about eluting species. This is an invaluable feature for field instrumentation, which has motivated the implementation of microsensor arrays as detectors in portable and micro-GCs.[15–17]

The limited sensitivity of most detectors precludes their directly monitoring VOCs in many applications of interest (*e.g.*, indoor air quality, breath biomarker analysis, ambient air monitoring), where concentrations in the low- or sub-parts-per-billion (ppb) range are common.[28–32] The latter problem has led to increasing use of SPME[33] or similar extrinsic preconcentration methods[10] prior to injection in order to reduce detection limits. On-board preconcentration is apparently not available as a standard component of many portable GCs.[9]

Several years ago, we reported on a first-generation portable GC prototype that incorporated a miniature, multi-stage adsorbent preconcentrator/injector (PCI) with a tandem-column separation module and a detector consisting of an array of polymer coated surface-acoustic-wave (SAW) microsensors.[34] That prototype was capable of quantitatively analyzing up to 30 VOCs at low- and sub-part-per-billion levels in a period of 10 minutes. The PCI was designed to increase the effective concentrations of trapped vapors spanning a wide range of vapor pressures and to inject samples by thermal desorption directly onto the first column. By carefully determining the minimum

[a]*Department of Environmental Health Sciences, University of Michigan, 109 S. Observatory, Ann Arbor, MI, 48109-2029, USA. E-mail: ezellers@umich.edu*
[b]*Department of Chemistry, University of Michigan, Ann Arbor, MI, 48109-2029, USA*

† Electronic supplementary information (ESI) available: the response patterns for all 31 compounds. See DOI: 10.1039/b810944c

quantities of adsorbents required, it was possible to avoid losses of vapors due to breakthrough of the adsorbent beds while also avoiding the need for downstream focusing prior to injection into the separation module.[35,36] Two columns in series, each with a different stationary phase, independent at-column temperature programming, and a pressure equalization bypass at their juncture for flow control, imparted the capability for 'tuning' the retention of eluting species thermally and pneumatically. Response patterns derived from the array of SAW sensors, coupled with retention times, facilitated the determination of the identities of eluting species, even where full chromatographic resolution was not achieved. The first-generation instrument was also successfully tested in a chamber study.[37]

Although these previous efforts established an unprecedented capability for trace-level determinations of fairly complex VOC mixtures with a portable GC, and confirmed the value of coupling tunable retention with sensor-array pattern recognition, there were several features of the instrument that required further optimization, including a more versatile temperature-programming capability (formerly limited to 3 step-wise increments), more effective chassis cooling, thermostatting of the sensor array, split-flow injection to reduce injection band broadening, a means of performing field calibration, improved detector sensitivity, and an alternative to the on-board microcontroller, which was somewhat cumbersome to use and which suffered from drift in its reference voltages.

The instrument described here retains the use of scrubbed ambient air as the carrier gas, and the same multi-stage PCI and dual-column separation modules. An alternative sensor technology is employed, however, comprising an array of chemiresistors (CR) coated with thiolate-monolayer-protected gold nanoparticles (MPNs) as interface layers, which purportedly provides higher signal-to-noise ratios.[15,30,38] Other enhancements in design include thermoelectrically (TE) cooling the sensor array, split-flow injection, an on-board calibration-vapor generator, and instrument control *via* a LabVIEW program run from a laptop computer.

In a recent preliminary study, this second-generation instrument was used to determine two environmental tobacco smoke (ETS) markers at sub-ppb concentrations in the presence of common indoor-air co-contaminants.[30] This article presents a thorough characterization of the second-generation instrument. Since the topics of preconcentrator design and pressure-tuned separations have been covered in previous articles,[30,34–36,39] they are not emphasized here. Rather, an emphasis is placed on the influence of changes in flow rate and temperature on the performance of the CR array. Neither of these topics has been explored previously for microsensor arrays used as GC detectors. Integration of the unique components and functions of this prototype to effect multi-vapor determinations is illustrated.

Prototype description and experimental methods

Instrument features and operating modes

Fig. 1 presents photographs of the interior and exterior of the instrument and diagrams of the analytical train in two of its four operating modes. It operates on ac power and has two on-board ac/dc (60 Hz/120 V) converters. The sequencing of functions is controlled by a laptop computer running routines written in LabView 7.1 (National Instruments, Austin, TX). Air flow is provided by one of two small diaphragm pumps (UN86KTDC, KNF Neuberger Inc., Trenton, NJ) and is directed by four solenoid-actuated diaphragm valves (NResearch Inc., West Caldwell, NJ). All exposed valve surfaces are Teflon-coated. Five miniature axial fans were added to dissipate heat generated within the instrument during normal operation (note: there were only two fans in the previous prototype).

The instrument proceeds through a sequence of up to four user-programmable operating modes. In Sampling Mode (Fig. 1a), air is drawn by the on-board sampling pump through an externally mounted Teflon-membrane particulate filter (47-mm, 1.0-μm pore, polypropylene cassette, SKC, Eighty Four, PA) and then through the PCI at an adjustable flow rate of up to 0.16 L/min. Vapors are captured on the three PCI adsorbents contained in an insulated, thin-walled Inconel 600® tube (1.35 mm i.d., 5-cm long) (Accu-tube Corp., Englewood, CO). For this study, the PCI tube was packed, in order, with 8 mg of 40/60-mesh Carbopack B, 2.5 mg of 40/60-mesh Carbopack X, and 1.8 mg of 45/60-mesh Carboxen 1000 (separated by glass woo1), which have specific surface areas of 100, 250, and 1200 m^2/g, respectively (Supelco, Bellefonte, PA).[36] The adsorbent masses used here were determined on the basis of a previous breakthrough study to have sufficient capacity for a 1-L sample containing over 40 compounds, each at 100 ppb.[36]

An on-board calibration-vapor generator (Microsensor Systems, Inc., Bowling Green, KY) was added as a quality control measure to assist in diagnosing uncompensated changes in ambient temperature or pressure, drift in flow rates or temperatures, leaks, and malfunctions in system components. The generator consists of a small vial packed with glass wool that is connected at one end to the inlet flow path through a 2-way solenoid valve (Fig. 1a) and at the other end to the exhaust port of a dedicated mini-diaphragm pump. A small volume of liquid calibrant (user selectable) is injected onto the glass wool and the vial is sealed to produce a saturated atmosphere. Brief actuation of the valve and pump dispenses a small amount of the headspace vapor into the inlet flow stream for capture by the downstream PCI. The scheduling of calibration-vapor injections can be defined by the user.

After sampling a pre-set air volume, the sampling pump is turned off and isolated from the system by an upstream valve. An optional dry-air purge (Purge Mode) can then be performed in which the analysis pump draws ambient air in through a second inlet port and passes it through a scrubber cartridge located inside the instrument. The scrubber is packed with charcoal and 4A molecular sieves to remove VOCs and water vapor, respectively. The purified air is directed through the PCI and out through the sample inlet port, and serves to remove a portion of the water from the PCI adsorbents and to backflush residual VOCs from the fore line. In a typical sequence, the Purge Mode duration is about 60 sec.[34,36]

In Analysis Mode (Fig. 1b), the inlet valve is closed and ambient air drawn into the system by the analysis pump is scrubbed and then directed through the PCI, the separation columns, and the detector cell prior to being exhausted from the instrument. After a 40-sec pressure stabilization period, the PCI is heated with an insulated Cu-wire coil to 300 °C in < 2 sec and

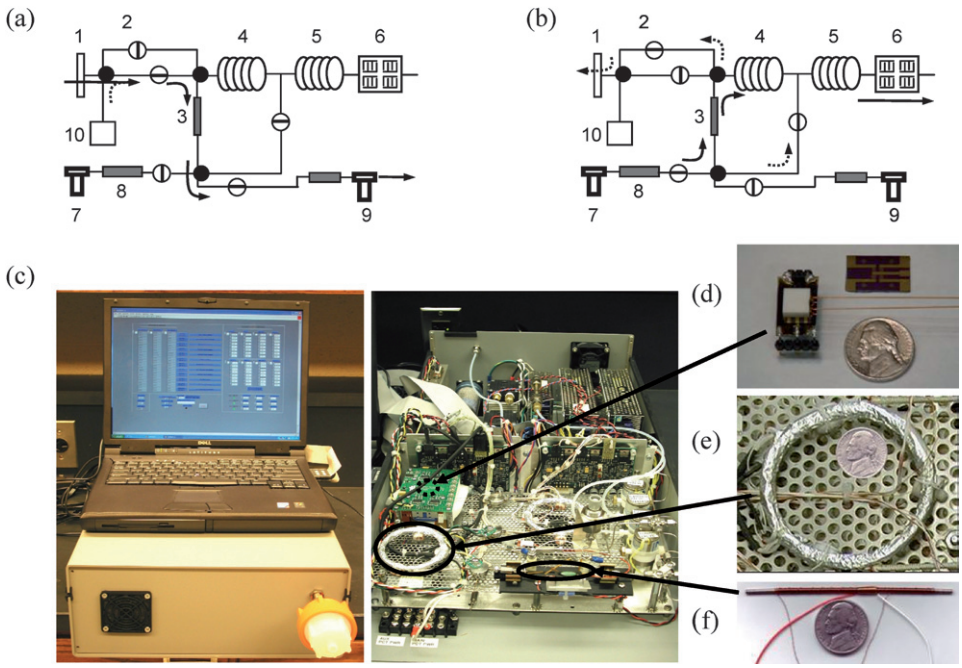

Fig. 1 Block diagrams and photos of the prototype portable GC and its key components: Arrows in diagrams depict flow paths during: (a) Sampling Mode and (b) Analysis Mode (dashed lines indicate optional flows); (c) photos of the prototype beneath a laptop PC (left) and with the cover removed (right); (d) CR array prior to adding electrical connections or lid (top right) and assembled with Macor lid (white square structure), inlet/outlet capillaries, and soldered header pins for electrical connection to the underlying PC board; (e) column wrapped with heater wire and thermocouples; (f) assembled PCI with heater and thermocouple. Components in the block diagram: 1 inlet filter, 2 split-flow control valve, 3 PCI, 4 1st column, 5 2nd column, 6 CR array, 7 analysis pump, 8 scrubber, 9 sample pump, 10 calibration-vapor generator.

maintained at this temperature for up to 90 sec. A type-K thermocouple wrapped in a thin sheath of polyimide tape and held against the PCI wall by the Cu wire was used for temperature feedback. The captured vapors are thereby thermally desorbed and injected into the first of the two separation columns. A split-injection capability was incorporated in this prototype to reduce injection plug width by venting a portion of the desorbed flow stream.[15,39]

The first separation column (4.5-m long, 0.25-mm i.d.) contains a wall-bonded polydimethylsiloxane stationary phase (DB-1, 0.5-μm thickness, Agilent, Wilmington, DE) and the second column, which has the same dimensions as the first, contains a wall-bonded polytrifluoropropylmethylsiloxane phase (RTX-200, 0.25-μm thickness, Restek, Bellefonte, PA). The moderately polar nature of the RTX-200 provides retention properties that complement those of the non-polar DB-1 phase.[40,41] The columns are heated independently using coiled 'at-column' heaters,[11,34] (note: the dual-column assembly was provided for this project by RVM Scientific Inc., Santa Barbara, CA). A bypass line shunts flow around the first column when the junction-point tuning valve is open, which stops the flow in the first column while accelerating the flow through the second column. This valve can be opened for short periods of time during an analysis to separate compounds that are resolved on the first column but would otherwise converge and co-elute from the second column.[34]

Eluting vapors are detected by the CR array, which consists of four sets of interdigital Au/Cr electrodes patterned on a single oxide-coated Si substrate. Each CR device contains 20 pairs of electrodes 0.40 μm thick, and 15 μm wide with a 15 μm spacing and a 1.4 mm overlap. Header pins bent at a 90° angle were soldered to the gold bonding pads and inserted into header sockets on a custom printed-circuit board (PCB) with multiple analog circuit trains for measuring resistance. A TE cooler and RTD temperature sensor were fixed to the lid of the detector cell with thermally conductive epoxy for control of the array temperature *via* a simple, manually set, feedback controller (MPT-5000, Wavelength Electronics, Bozeman, MT).

Each CR sensor is coated with a different solvent-cast film of a gold-thiolate monolayer protected nanoparticle (MPN).[15,38,42] Film thicknesses were estimated to be ~200 nm, assuming 3 g/mL density.[42] The coated array is capped with a Macor® lid (cell volume ~ 3 μL) and fitted with inlet and outlet capillaries for fluidic interconnections. The cap is held in place with a patterned rectangular gasket of tape with adhesive on both sides that is 127 microns thick (VHB tape, 0.005 inch thickness, 3M, St. Paul, MN). MPNs derived from the following thiols were used in this study: n-octanethiol (C8), 1-mercapto-6-phenoxyhexane (OPH), 7-mercaptoheptanitrile (CCN), methyl 6-mercaptohexanoate (HME), and 4-mercaptodiphenylacetylene (DPA).[30,43] A constant dc bias is applied to each sensor and the current is converted to a voltage, baseline corrected, amplified, and recorded with a data acquisition card on a laptop computer.

In the CR array, vapors reversibly partition into each MPN film and cause it to swell, which changes the electron tunneling barrier and thereby the film resistance.[42,44] Since the structures of the MPN ligands differ on each sensor, the affinities for a given vapor differ as well, and the array of CRs produces a different set of responses for each vapor. Over the course of this study, several different arrays were installed in the instrument, depending on

the particular issue being examined. For some tests, only a single sensor in the array was coated and used for data collection. Baseline RMS noise levels varied with the MPN film but were typically on the order of 10–20 mV.

Following detection, the PCI is re-conditioned by sequentially heating (300 °C) and backflushing with scrubbed air for 60 sec, and then cooling actively with on-board fans prior to collecting the next sample. Assuming a 1-L sample volume and a 5-min separation, an entire analytical cycle (including post-sample PCI purge and cooling) can be completed in 16 min.

Software written in house is run from a laptop computer and used to control the instrument and process the sensor output signals through separate 12 bit and 16 bit data acquisition cards (Measurement Computing Corp., Middleboro, MA) at a rate of ≥ 50 Hz. The output voltages from the sensors are recorded in a text file and converted to chromatograms with Grams 32 software (Thermogalactics, Inc., Salem, NH). Peaks were integrated with Grams following smoothing using 40-point running average.

Materials and test atmosphere generation

Test atmospheres of the vapors were generated by injecting small volumes of the liquids into 12-L Tedlar® bags (SKC, Eighty-Four, PA) prefilled with a known volume of clean, dry air from a compressed-air cylinder. Concentrations were confirmed *via* GC-FID by comparison with injected masses of CS_2 solutions of the same compounds. For compounds with very low vapor pressures, a saturated test atmosphere was created in a 1-L Tedlar bag and aliquots were transferred by gas-tight syringe to a series of other bags or injected directly into the inlet of the instrument. Methane was used for testing column hold-up times.

Instrument calibration and chemometrics

Conditions required to separate a 31-component mixture in a minimum amount of time were established using external sample loops with volumes ranging from 0.01–1 mL to cover the desired range of injected masses. Effective (mass-equivalent) vapor concentrations were calculated according to the ratio of injection and sample volumes. For example, an aliquot of 1 mL from a sample loop containing 10 ppm of vapor is equivalent to 10 ppb in a 1-L sample volume. Mass-equivalent calibration concentrations ranged from 0.15–150 ppb-L. Four replicates were performed for each of seven challenge concentrations within this range for each of the 31 compounds.

Chemometric analyses of sensor array response patterns were performed using Monte Carlo simulations in conjunction with extended disjoint principal components regression (EDPCR) to estimate expected recognition rates for the components of co-eluting mixtures.[45,46] Monte Carlo simulations superimpose random error on calibrated sensor-array response patterns, which are then classified by EDPCR to determine if the co-eluting components giving rise to the composite response pattern can be recognized and discriminated with low error.[46] In the Monte Carlo error model, experimental values of RMS baseline noise were used and errors in sensitivities within the range of 1–8% were used, depending on the sensor. Iterative analysis (n = 500) over a predefined range of concentrations yields statistical estimates of discrimination.

Results and discussion

Basic operation

In the previous prototype, event sequencing and set points were controlled by an embedded microcontroller. As the chassis temperature increased, the reference voltages for the column temperatures and carrier gas inlet pressure drifted from their initial settings. As a result, retention times would increase over time from cycle to cycle. This problem was solved in the current prototype by removing the microcontroller and shifting control to the laptop computer. Highly stable flow rates, column temperatures, and retention times, t_R, were achieved.

To test the sampling and desorption functions, the sensor array was bypassed and replicate samples of n-octane were analyzed using an FID. Peak areas were reproducible to within 4% (RSD) with splitless injection and to within 6% (RSD) with a 6:1 split injection (n = 6). Similar testing of the vapor generator, using n-decane as the calibrant yielded peak area variations of 10% (RSD, n = 10). This reflects some variability in the quantity of vapor injected from the generator assembly, which may be related to the lack of temperature control on the reservoir.

Owing largely to the ability of the TE cooler to maintain the array temperature to within 1 °C of its set-point temperature, peak-area sensitivities are quite stable in the short term, varying by only 4–7% over 20 continuous analytical cycles (toluene) for an array coated with C8, OPH, DPA, and HME MPNs. Over a period of two months, however, periodic calibrations revealed that sensitivity values would drift by as much as 60%, and the HME-coated device showed a consistent gradual decline in sensitivity. With the exception of this sensor the drift in sensitivities was cyclic and similar for all sensors. There was enough of a difference, however, to cause significant changes in relative response patterns. Such variations in MPN-coated CR sensors have been noted in the literature,[42] and appear to be related to changes in the inter-particle distances within the cast films. The practical implication of this phenomenon is that re-calibration of the instrument and re-establishment of the response pattern library would be needed roughly every two weeks.

Column efficiencies

The chromatographic efficiency of each column was determined independently using n-octane samples loaded onto the PCI and injected with a split ratio of 4.4:1. An FID detector was used for these tests. Golay plots yielded values of the minimum plate height, H_{min}, of 0.027 and 0.051 cm for the first and second column, respectively. The corresponding maximum plate counts, N, are 3,700 and 2,000 plates per metre, respectively. Plotting the rate of plate production per unit time as a function of average velocity indicates that the optimum practical gas velocity (OPGV) is ~25 cm/s, which corresponds to a volumetric flow rate at the dual-column outlet of ~0.8 mL/min at 30 °C. This is 2.8 times the optimal velocity and results in a ~2-fold increase in H.

Extracolumn band broadening

Contributions to band broadening from adsorbent preconcentrators similar to that used here have been studied

previously.[15,19,34,39] Rapid heating rates and high flow rates through a PCI serve to minimize broadening, but analyte volatility is also an important co-factor. Band broadening from the type of microsensor array used here has not been studied systematically,[15] and could arise from the finite volume of the detector cell as well as the rates of sorption and desorption of eluting vapors into and out of the interface layers on the sensors. Adsorption on unheated interconnection surfaces may be significant for less volatile analytes (*vida infra*).

Golay plots were constructed for n-nonane using data generated with the PCI (splitless) and then with a heated 0.1-mL sampling loop injector connected *via* a heated 6-port valve to the inlet of the first column (valve and sample loop = 180 °C; k = 4.9; FID). Values of H_{min} were 0.068 and 0.10 cm for the loop and PCI, respectively. The Golay plot constructed for n-nonane using data generated with the sensor array operated at 23 °C (loop injector) was nearly superimposable on that obtained using the FID, yielding a value of H_{min} of 0.071 cm (OPH-coated sensor). Consistent with this, the average ratio of peak widths at half height, $W_{1/2}$, (*i.e.*, OPH:FID) was 1.1.

Subsequent tests with C_{10}–C_{12} n-alkanes gave OPH:FID $W_{1/2}$ ratios of 1.1 1.4, and 2.4, respectively, indicating that peak widths for compounds less volatile than n-decane become significantly broader with the sensor(s). Among the different sensors in the array, $W_{1/2}$ values for these n-alkanes were generally in a ratio of 1:1:1.1:1.2:1.2 for sensors coated with C8, OPH, HME, CCN, and DPA MPNs, respectively. The small increase in peak width observed for the MPNs with polar tail groups may be due to longer diffusion times or possibly to longer film relaxation times arising from the stronger inter-ligand interactions extant in films of these MPNs.

Split-flow injection

Although less-volatile compounds can be focused at the head of the separation column if it is initially at low temperature, such focusing is not possible for isothermal separations or for compounds having vapor pressures above a few torr without actively cooling the column.[36] Since the heating rate of the PCI could not be increased further, only the carrier gas flow rate through the PCI was explored as a means of reducing the injection band width. Split-flow injection has been shown to improve resolution in portable and micro-scale GCs,[15,39] at the expense of sensitivity. However, the former is often the more important factor in complex mixture analysis. In its current configuration the split ratio is determined by the relative resistances of the analytical and vent flow paths and was limited to ~7:1.

Results of one representative series of tests are summarized in Table 1 and Fig. 2 for a mixture of C_7–C_{12} n-alkanes (22 to 37 ppb-L injected) tested at a split ratio of 6.6:1 and an outlet flow rate of 0.7 mL/min, which corresponds approximately to the OPGV (column temp. = 90 °C; FID). As expected, split-flow injection leads to reductions in $W_{1/2}$ and, consequently, to increases in column efficiency, N, and chromatographic resolution, R. Reductions in $W_{1/2}$ values range from 1.8-fold for n-heptane to 3.1-fold for n-dodecane, reflecting the greater influence of the desorption flow rate on less-volatile vapors. Although the resolution generally increases down the homologous series from C_7 to C_{12} (Table 1), as shown in Fig. 2 the values of t_R also decrease significantly for C_{11} and C_{12}; since R is proportional to $t_R/W_{1/2}$, the improvement in resolution for these compounds is less than what would be expected on the basis of $W_{1/2}$ alone.

At least a portion of the improvement in R is due merely to the reduced injection mass, which is nominally 13% of the splitless injection mass. To explore whether the split-flow injection was improving R beyond that afforded by this factor, all peaks were modeled as triangles and the measured peak height and peak area were used to calculate a 'reference value' of $W_{1/2}$. Comparing the reference value to the actual value of $W_{1/2}$ provided a means of assessing the peak width while controlling for injection mass. On the basis of such comparisons it appears that for C_7–C_{10} the decrease of $W_{1/2}$ is due almost entirely to the decrease in injection mass, while for C_{11} and C_{12} the decrease of $W_{1/2}$ exceeds that attributable to the decrease in injection mass alone by about 12 and 22%, respectively.

Peak areas for the C_7–C_{10} alkanes with split-flow injection are ~12% of those under splitless conditions, which is roughly consistent with the split ratio. For C_{11} and C_{12}, the peak area ratios are 0.14 and 0.17, respectively. This can be ascribed to the desorption efficiency (recovery) of these relatively low-volatility vapors being higher with split-flow injection than with splitless injection. Assuming 100% desorption efficiency with the split injection, the corresponding desorption efficiencies for splitless injection of C_{11} and C_{12} are approximately 85% and 72%, respectively. Separate tests confirmed residual quantities of these compounds in amounts consistent with these estimates of desorption efficiency.

These results concur with earlier reports showing that the relative gain in resolution is less than the relative loss in sensitivity when using split-flow injection.[15] In this study, 2–3–fold increases in resolution are accompanied by 6–8-fold reductions in sensitivity. Furthermore, for the shorter alkanes, the increase in resolution can be ascribed almost completely to the reduced mass of the split injection. In addition, these results show that for compounds more volatile than n-undecane the injection band width from a PCI is limited by the heating rate of the PCI, whereas for less volatile vapors the band width is also affected by the flow rate through the PCI.

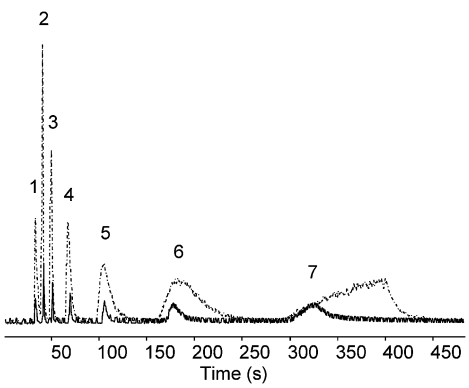

Fig. 2 Chromatograms illustrating the effect of split-flow PCI injection on peak shape and resolution (FID). Solid trace is for split injection (6.6:1) and dashed trace is for splitless injection. Compounds: 1 methane; 2 n-heptane; 3 n-octane; 4 n-nonane; 5 n-decane; 6 n-undecane; 7 n-dodecane.

Table 1 Ratios of various chromatographic performance parameters (split:splitless PCI injection) illustrating the tradeoff between sensitivity and resolution

	Ratio of parameter value[a]						
Compound	$t_{R\text{-}S}/t_{R\text{-}NS}$	A_S/A_{NS}	H_S/H_{NS}	LOD_S/LOD_{NS}[b]	$W_{1/2\text{-}S}/W_{1/2\text{-}NS}$	N_S/N_{NS}[c]	R_S/R_{NS}[d]
n-heptane	1.0	0.12	0.21	4.8	0.54	3.5	2.0
n-octane	1.0	0.12	0.23	4.3	0.50	4.2	2.2
n-nonane	1.0	0.12	0.28	3.6	0.45	5.3	2.7
n-decane	1.0	0.12	0.34	2.9	0.35	8.5	2.7
n-undecane	1.0	0.14	0.40	2.5	0.32	8.9	2.1
n-dodecane	0.8	0.17	0.40	2.5	0.33	6.0	—

[a] t_R is retention time, A is peak area, H is peak height, $W_{1/2}$ is peak width at half height, N is total plate count, and R is resolution; subscript S denotes split injection; subscript NS denotes splitless injection. Column outlet flow rate was 0.7 mL/min and split ratio was 6.6:1 in all cases. [b] LOD = 3σ/(peak-height sensitivity), where σ is the RMS baseline noise. [c] $N = 5.45\ (t_R/W_{1/2})^2$. [d] $R = 1.18(\Delta t_R/(W_{1/2(n)} + W_{1/2(n+1)}))$ determined between the indicated n-alkane and its next higher homologue.

Flow rate effects on detection

Among the distinguishing features of the MPN-coated CR array as a GC detector is that the sensor responses depend on the vapor concentration (mass/volume) in contrast to an FID, whose response depends on mass/time. This feature of the CR array allows for miniaturization without loss of sensitivity because the response depends on partitioning of vapors into the interface layer.[42] However, since bands eluting from the column have a finite residence time in the detector cell, kinetic factors must be considered. Fig. 3 shows the effect of flow rate on the peak width, height, and area for n-octane and n-nonane from the

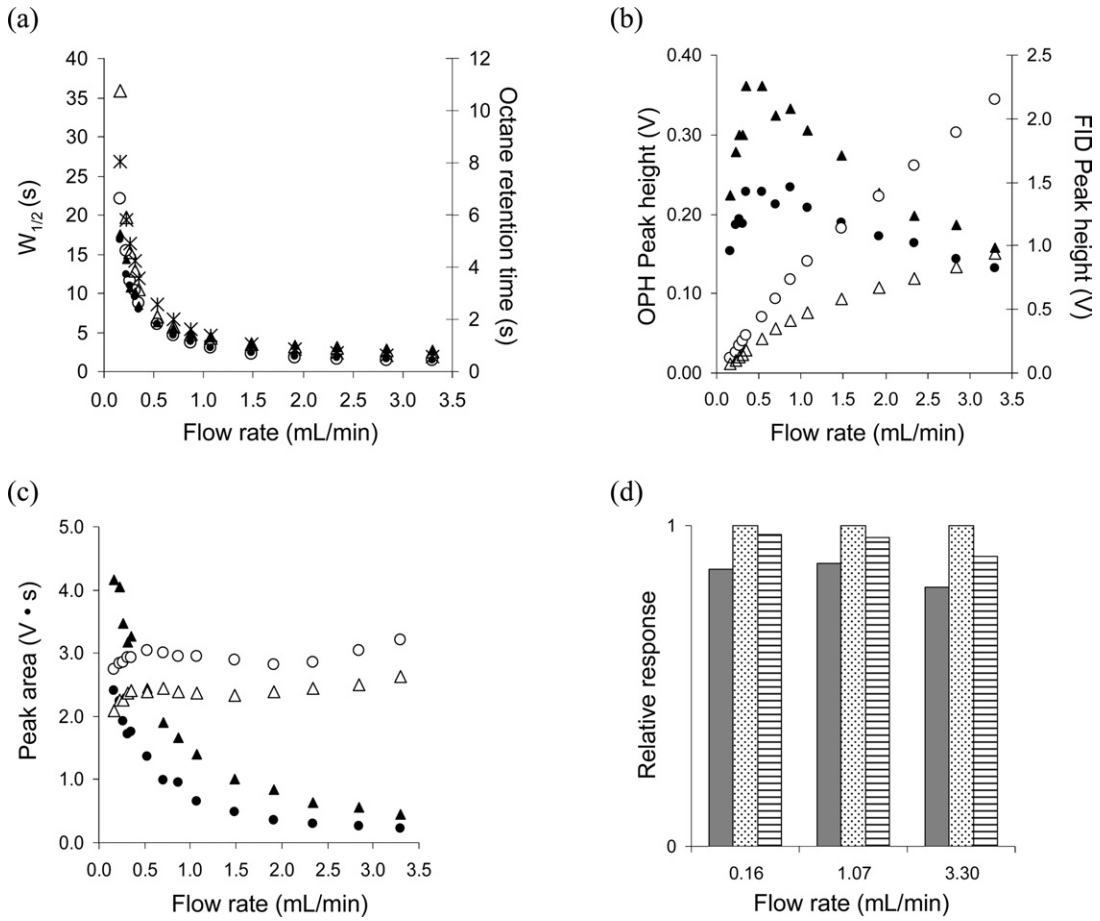

Fig. 3 Effects of carrier gas flow rate on peak parameters from the CR sensors and an FID: (a) Peak width at half height and n-octane retention time versus outlet flow rate; (b) Peak height versus outlet flow rate; (c) Peak area versus outlet flow rate; (d) Response patterns of n-octane at different flow rates. Legend: filled circles: n-octane from OPH; unfilled circles: n-octane from FID; filled triangles: n-nonane from OPH; unfilled triangles: n-nonane from FID; stars: n-octane retention time. For the bar chart, from left to right at each flow rate: C8, OPH, and DPA sensors. The 0.1 mL heated sample loop was used and the amount injected was 156 ng (*i.e.*, 50 and 70 ppb-L for n-octane and n-nonane, respectively).

OPH-coated sensor and from an FID placed immediately downstream from the CR array.

Values of $W_{1/2}$ decrease sharply at first and then more gradually with increasing flow rate to a similar extent for both vapors with both detectors. Values of t_R decrease in direct proportion to the decreases in $W_{1/2}$, as shown in Fig. 3a for n-octane. The peak height passes through a maximum for both vapors with the sensor but steadily increases for both vapors with the FID. The peak area decreases in a manner similar to that of $W_{1/2}$ but less sharply at the lower flow rates for both vapors with the sensor, and it is nearly invariant for both vapors with the FID. All sensors behaved similarly.

To interpret these results it is important to recognize that the responses of the sensors and the FID are affected by the changes in the injection bandwidth and the time on the column accompanying changes in flow rate through the system. Over the range of flow rates examined the retention times of n-octane and n-nonane decrease by about 19-fold. In general, the less time a compound spends on the column the less band dispersion that occurs and the narrower its peak. Another factor to consider is the reduction in the vapor concentration accompanying the higher flow rate during desorption. The finite (dead) volume of the detector cell may also contribute to broadening at lower flow rates. The peak width is expected to decrease with increasing flow rate due to all of these factors, and the shapes of the $W_{1/2}$ curves in Fig. 3a are consistent with the superposition of such factors. In fact, it appears that the decrease in $W_{1/2}$ can be attributed almost entirely to these factors, since similar behavior is seen for both types of detectors and both vapors.

The flow rate dependence of the peak height for the sensors is consistent with this interpretation (Fig. 3b). At low flow rates there is a roughly linear increase in peak height, which can be ascribed to peak sharpening accompanying the retention time decreases and the diminishing influence of the detector dead volume. At about 0.35 mL/min for both vapors, however, a plateau is reached and at higher flow rates the trend reverses and the peak heights gradually decline due to the dilution effect becoming dominant. Note that the overall change in peak height is small: the ratio of maximum-to-minimum peak height is only ~2 and the RSD is only 17% and 24% for n-octane and n-nonane, respectively.

For the FID, the peak height also increases linearly up to about 0.6 mL/min for both vapors and then continues to increase but at a steadily declining rate for both vapors. That is, the peaks continue to become sharper over the entire flow rate range, reflecting the increase in mass/time measured by the FID, but at a decreasing rate over the range in which the sensor(s) exhibit a decreasing height due to a decrease in mass/volume. This indicates that the peaks get sharper at a rate exceeding that at which they are being diluted, such that the mass/time continues to increase in spite of the decrease in mass/volume. The relative magnitude of the effect on the FID peak height is similar for both vapors. The difference in behavior between the concentration-dependent sensor and the mass-sensitive FID is quite dramatic.

For the sensor(s), the peak area decreases at a high rate at first and then more gradually at the higher flow rates (Fig. 3c). A plot of peak area versus (flow rate)$^{-1}$ is linear out to a value of ~2.0 (flow rate ~0.5 mL/min), at which point the slope decreases. This indicates that a factor other than carrier gas dilution is affecting the peak area, which we believe to be dilution arising from the detector dead volume. The lack of a significant change in peak area from the FID reflects the countervailing influences of the decrease in $W_{1/2}$ and the increase in peak height.

Fig. 3d shows the relative response pattern for n-octane at three flow rates: the lowest, highest, and mid-range values. Some variations are observed, but they are not significant and can be attributed to normal variations in sensor responses. The responses for the polar CCN-coated sensor to this alkane vapor were quite low and quite variable due to the effects of baseline noise, so they were omitted from the patterns in Fig. 3d. These results confirm that the flow rate effects are similar for all of the sensors.

A possible alternative explanation for these trends in peak width and peak height is that the sorption/desorption kinetics of the vapors in the MPN films become slow relative to the residence time of the vapor in the detector cell as the flow rate increases. However, using reasonable estimates of diffusion coefficients in air and in the MPN films,[47–50] diffusion times are ~0.020 sec, whereas residence times in the detector cell range from 0.05 to 1 sec for flow rates of 3.3 to 0.16 mL/min, respectively. Thus, it is not likely that these kinetic factors are influencing the peak parameters and behaviors depicted in Fig. 3.

The practical implications of the results are significant. At low flow rates the peak area is extremely sensitive to flow rate, such that a change of 0.1 mL/min can lead to a change in peak area of 20% for the example shown in Fig. 3 at flow rates in the range of 0.1–0.3 mL/min. This demands tight control on flow rate in this regime. At higher flow rates the dependence is greatly reduced, but so is the sensor response (*i.e.*, sensitivity). Most subsequent experiments in this study were performed at a flow rate of 0.8–1.0 mL/min, which represents a compromise between these two factors. The relatively weak dependence of peak height on flow rate for the sensors facilitates establishing LODs, since LODs are determined from peak-height sensitivities.

Temperature effects on detection

As shown above, although $W_{1/2}$ values from the FID and the CR sensors in the array are comparable for the more volatile compounds, those from the sensors are much broader for the less volatile vapors than those from the FID under the same separation conditions. Factors that would contribute to broader signals from the sensor array for these vapors include smaller diffusion coefficients and adsorption on surfaces in the flow path. Since diffusion coefficients do not differ greatly across this range of compounds (*i.e.*, at 23 °C, for C_9 to C_{12} the diffusion coefficients in air range from 0.055 to 0.048, respectively, and at 43 °C, they range form 0.061 to 0.053, respectively)[47] diffusion rates alone cannot account for the degree of peak broadening observed for the less volatile compounds in this series, and it is likely that other factors are affecting the mass transport process. Regardless, by increasing the temperature of the sensor array, the rates of all relevant processes should increase which, in turn, should decrease $W_{1/2}$. Since the vapor-film partition coefficient, K, should have an Arrhenius-type temperature dependence,[51] it will also decrease, and there will be a tradeoff between resolution and sensitivity.

A mixture of C_9–C_{12} n-alkanes was analyzed at each of five sensor temperatures from 23–43 °C. Injections (62–144 ng;

Table 2 Ratios of various chromatographic performance parameters at different sensor-array temperatures illustrating the tradeoff between sensitivity and resolution[a]

		compound			
Parameter Ratio [b]	T_1 (°C)	n-nonane	n-decane	n-undecane	n-dodecane
$W_{1/2\text{-}T1}/W_{1/2\text{-}T2}$	25.6	1.00	0.97	0.87	0.85
	30.5	0.94	0.84	0.70	0.63
	37.9	—	0.80	0.65	0.48
	42.7	0.88	0.79	0.59	0.46
N_{T1}/N_{T2}	25.6	1.01	1.06	1.32	1.38
	30.5	1.14	1.42	2.06	2.52
	37.9	—[c]	1.54	2.35	4.43
	42.7	1.29	1.59	2.91	4.76
A_{T1}/A_{T2}	25.6	0.90	0.84	0.89	0.96
	30.5	0.66	0.57	0.59	0.62
	37.9	—	0.46	0.38	0.34
	42.7	0.43	0.32	0.22	0.20
H_{T1}/H_{T2}	25.6	0.77	0.86	0.91	0.98
	30.5	0.67	0.62	0.60	0.72
	37.9	—	0.51	0.38	0.47
	42.7	0.47	0.35	0.23	0.27
R_{T1}/R_{T2}[d]	25.6	1.00	1.08	1.12	—
	30.5	1.09	1.21	1.31	—
	37.9	—	1.30	1.52	—
	42.7	1.15	1.33	1.62	—

[a] Data are from the OPH-coated CR sensor. [b] $T_2 = 23$ °C. [c] An accurate value could not be obtained due to excessive noise in the data channel. [d] Resolution between the indicated n-alkane and its next higher homologue.

17–28 ppb-L; splitless) were made with the PCI and the columns were temperature programmed to accelerate the separations. Results from the OPH-coated sensor are summarized in Table 2 and reveal the expected trends; values of $W_{1/2}$ decrease by 1.1–2.4-fold over the temperature range, with a larger change for the less volatile compounds, and the peak areas decrease by 2.3–5-fold, again with the effect being more prominent for the less volatile compounds. Increases in N range from 1.1 to 4.8-fold which is consistent with the dependence of N on the inverse square of $W_{1/2}$. Peak height and peak area track each other quite closely. Overall, as with the split flow experiments, the fractional gain in resolution is about half the fractional loss in sensitivity.

As with the split-flow experiments the decreases in $W_{1/2}$ can be attributed, at least in part, to the decreased mass uptake by the MPN films at higher temperatures. Modeling the peaks as triangles again, a reference value of $W_{1/2}$ was calculated for each peak under all conditions. Taking the ratio of the reference $W_{1/2}$ to the actual $W_{1/2}$ permits an assessment of peak narrowing that controls for the reduction in sorbed mass. From such an analysis it was determined that for n-octane and n-decane the decrease in $W_{1/2}$ beyond that due to the mass reduction was < 15%, while for n-undecane and n-dodecane, the fractional changes were 37% upon increasing the array temperature by 20 °C.

Analysis of a complex VOC mixture

One of the primary advantages of sensor array detection is the use of response patterns to identify compounds co-eluting from the separation module.[34,45,46] However, in cases where the number of co-eluting compounds exceeds three or where the co-eluting compounds have similar response patterns, errors in recognition can occur. By use of the pressure tuning and temperature programming features of the separation module, the capabilities of the array detector can be used to best advantage.

To illustrate this functional integration of the system components, a mixture of 31 organic compounds comprising common indoor and outdoor contaminants from several functional-group classes,[52] which collectively span a 1700-fold range of vapor pressure, was analyzed. The compounds have been assigned numbers and are listed in Table 3. A CR array freshly coated with the following MPN films was installed: C8, OPH, HME, and CCN. Using splitless PCI injection and an outlet flow rate of 0.9 mL/min, an initial separation was attempted using the same temperature program for both columns. The representative chromatogram from the C8 sensor presented in Fig. 4a shows that there are five binary co-elutions (*i.e.*, compounds 5/6, 14/15, 24/25, 27/28, and 29/30) and one ternary co-elution (*i.e.*, compounds 20/21/22). By maintaining the same temperature program for the first column, but changing that for the second column the resolution improves such that there are only three binary co-elutions and one ternary co-elution (*i.e.*, 13/14, 21/22, 27/28, 23/24/25, respectively, Fig. 4b). This illustrates the value of independent temperature programming of the columns.

Table 3 Calibration data summary for the 31-vapor mixture

				LOD (ppb)[b]			
#	compound	p_v[a] (torr)	t_R (sec)	C8	OPH	HME	CCN
1	ethyl acetate	93.7	53	0.61	0.72	5.6	2.5
2	benzene	95.2	62	0.51	0.58	6.3	2.7
3	trichloroethylene	69	76	0.47	0.55	5.0	2.6
4	methyl cyclohexane	46	90	0.85	1.1	20	10
5	methyl isobutyl ketone	19.9	100	0.22	0.26	2.6	1.0
6	toluene	28.4	112	0.22	0.24	2.7	1.2
7	2-hexanone	11.6	127	0.20	0.21	2.0	0.88
8	tetrachloroethene	18.6	141	0.27	0.31	3.8	1.9
9	n-butyl acetate	11.5	147	0.18	0.21	1.8	0.90
10	chlorobenzene	12	164	0.11	0.11	1.4	0.61
11	ethylbenzene	9.6	178	0.11	0.11	1.5	0.65
12	m-xylene	8.29	185	0.12	0.13	1.6	0.69
13	3-heptanone	2.6	199	0.12	0.12	1.4	0.59
14	o-xylene	6.61	201	0.083	0.10	1.2	0.47
15	n-nonane	4.45	217	0.067	0.082	1.5	0.77
16	isopropylbenzene	4.5	225	0.065	0.070	1.0	0.40
17	α-pinene	4.75	237	0.24	0.29	6.1	2.3
18	n-propylbenzene	3.42	246	0.049	0.050	0.92	0.40
19	4-ethyl toluene	3	253	0.051	0.049	1.1	0.32
20	2-ethyl toluene	2.61	265	0.031	0.032	0.61	0.21
21	1,2,4-trimethyl-benzene	2.1	276	0.032	0.037	0.61	0.21
22	3-octanone	2	276	0.053	0.050	0.75	0.32
23	1,4-dichlorobenzene	1	286	0.035	0.036	0.69	0.17
24	sec-butylbenzene	1.75	288	0.027	0.028	0.58	0.20
25	n-decane	1.43	290	0.027	0.041	0.78	0.29
26	d-limonene	1.98	303	0.036	0.041	0.88	0.34
27	n-undecane[b]	0.412	329	0.0049	0.0055	0.14	0.04
28	acetophenone[b]	0.397	342	0.023	0.024	0.22	0.051
29	n-dodecane[b]	0.136	357	0.0039	0.0040	0.15	0.039
30	naphthalene[b]	0.085	374	0.11	0.089	2.1	0.41
31	n-tridecane[b]	0.0558	397	1.03	1.0	26	8.5

[a] vapor pressure at 25 °C from Ref. 53. [b] LODs were estimated by extrapolation of responses in the (linear) low-concentration range.

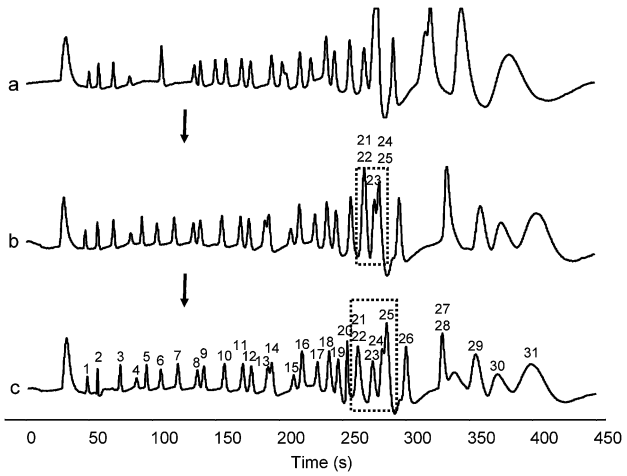

Fig. 4 Tuned separation of a 31-component mixture (C8 traces shown; numbers correspond to the compounds listed in Table 3): (a) both columns subjected to the same temperature program, starting 30 °C for 70 s, increased to 82.5 °C at 0.25 °C/s, then increased to 150 °C at 3.4 °C/s, hold; (b) two columns subjected to different temperature programs, which, for column 1 was the same as that in (a) and for column 2 was 50 °C for 70 s, increased to 100 °C at 1.0 °C/s, hold; (c) same temperature programs as in (b), but with pressure modulation consisting of opening the junction-point flow bypass valve at t = 242 s for 3 s and again at t = 252 s for 3 s.

The relative response patterns for the nine compounds that co-elute with at least one other compound are presented in Fig. 5. Visual inspection shows that the patterns of some co-eluants are quite similar, but that there are subtle differences between them that might permit their discrimination. Analysis by Monte Carlo simulation coupled with EDPCR classification models constructed for the nine individual compounds and their binary and ternary mixtures was performed over a concentration range of 1–5 × LOD for each compound. Disregarding any partial separations, the resulting estimates of the recognition rates were 96, 96, and 97% for the binary mixtures of 13/14, 21/22, and 27/28, respectively. That is, the statistical estimate of the ability to differentiate the mixture from its two components ranges from 96–97% for these mixtures. Using 95% recognition as a minimum threshold rate for satisfactory performance, these results indicate it would not be necessary to separate the binary mixtures because they could be resolved by use of pattern recognition. For the ternary mixture, on the other hand, the estimated recognition rate is only 87%. Therefore, the ternary mixture would require further separation to avoid confusing the mixture for one of the three possible binary component mixtures or one of the individual components.

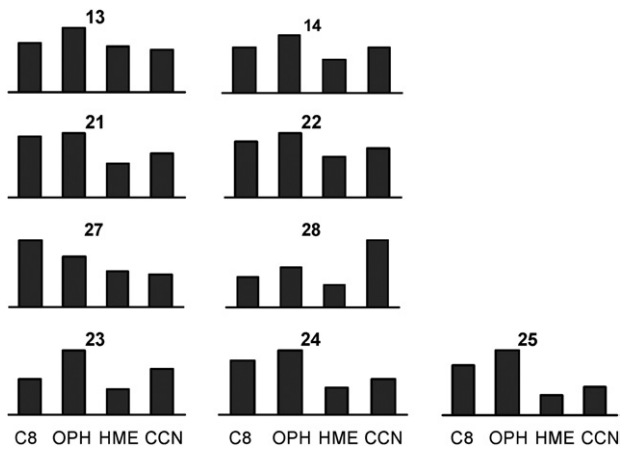

Fig. 5 Relative response patterns of compounds that co-elute in Fig. 4b (numbers correspond to the compounds in Table 3).

Fortuitously, compound 23 could be separated from compounds 24 and 25 by junction-point pressure modulation because these compounds are resolved on the first column. By opening the pressure-tuning valve for 3 s just after compound 23 has passed the column junction point (*i.e.*, at t = 242 sec), sufficient band separation is created to achieve complete resolution of compound 23 from the binary mixture of 24/25 at the outlet of the second column. EDPCR-Monte Carlo analysis yielded a recognition rate of 98% for the binary mixture of 24/25, so the problem was solved. An additional pressure modulation (for 3 sec at t = 252 sec) was required, however, to avoid the consequent co-elution of compound 23 with the compounds 21/22. As shown in the final trace of Fig. 4c, in a net separation time of seven minutes, 23 of the compounds are completely resolved and the remaining binary co-elutions can by differentiated/identified by use of pattern recognition. The traces from all four CR sensors under these conditions are presented in Fig. 6, and the response patterns for all 31 compounds are provided in the ESI.†

The chromatograms from the CR array sensors shown in Fig. 6 represent the best separation achievable in the minimum amount of time. For compounds 1–20, values of $W_{1/2}$ are < 3 sec for the C8 and OPH sensors and fractionally broader for the HME and CCN sensors. For the later-eluting compounds, peaks become significantly broader. Similar trends have been observed in our previous study of MPN-coated CR arrays as GC detectors and for polymer-coated SAW sensors arrays used as GC detectors in the first-generation instrument.[35,37] As in those previous studies, the $W_{1/2}$ values observed with the sensor and an FID are similar for early eluting compounds (data not shown), but are much broader from the sensors for the later-eluting compounds. Furthermore, if the FID is used downstream from the sensor array significantly broader peaks are observed than with the FID installed in place of the array. The available evidence suggests that wall adsorption in the array detector cell and on (unheated)

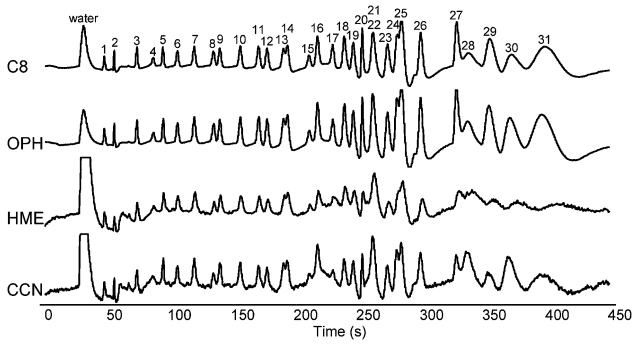

Fig. 6 CR-array chromatogram traces of the tuned separation of the 31-component mixture. Numbers correspond to the compounds listed in Table 3. GC conditions are the same as those in Fig. 4c.

interconnecting capillaries contributes significantly to the problem with less volatile compounds.

The instrument was calibrated with the 31 vapors under the separation conditions just established over a ~100-fold concentration range in each component by use of a series of Tedlar bags and different injection volumes. The vapor concentration ranges differed, depending on the sensitivities of the sensors to the compound, with lower concentrations (~0.1–10 ppb-L) being used for the later-eluting compounds whose responses were generally larger than those of the earlier-eluting (*i.e.*, more volatile) compounds (~3–300 ppb-L).

Plots of peak area (or peak height) versus sample quantity (in ppb-L) were linear for 25 of the 31 vapors on all four sensors (*i.e.*, for a forced-zero regression $r^2 > 0.95$, and in most cases $r^2 > 0.99$). Calibration curves for the five compounds with the lowest vapor pressures, *i.e.* n-undecane, acetophenone, n-dodecane, naphthalene, and n-tridecane (compounds 27–31 in Table 3) were nonlinear, with sensitivities decreasing at higher concentrations. This can be ascribed to a combination of wall adsorption on interconnecting components in the system and low desorption efficiencies from the PCI. For these compounds the LODs in Table 3 were extrapolated from the data at the lower concentrations.

The LODS generally decrease (sensitivities increase) with decreasing vapor pressure of the analyte as expected for sorption-dependent sensors (Table 3).[38,42] This trend is fairly consistent across all four CR sensors, though some exceptions are observed that can generally be attributed to the mitigating influence of vapor-MPN interactions. Note that the sensitivities of α-pinene, naphthalene, and n-tridecane are much lower than expected. For α-pinene, this was due to partial decomposition during thermal desorption, as evidenced by small additional peaks generated when analyzing this compound alone in separate tests. For naphthalene and n-tridecane wall adsorption and low desorption efficiencies were contributory. Naphthalene and n-tridecane notwithstanding, calculated LODs range from 3.9 ppt for n-dodecane (C8 sensor) to 20 ppb for methyl cyclohexane (CCN sensor), assuming a 1-L sample volume.

Compared to the earlier prototype, which employed an array of polymer-coated surface acoustic wave (SAW) sensors as the detector,[34] this instrument provides LODs that are from 3–55 times lower for the 17 compounds tested on both instruments. This can be ascribed to the higher inherent sensitivity[38] and better thermostatting of the CR sensor array, and more precise control of the temperature ramps in each separation column, which produces sharper peaks. The latter factor also leads to an increase in peak capacity compared to the earlier prototype, as evidenced by the larger number of fully resolved peaks in the 31-vapor chromatogram in a shorter amount of time.

Conclusions

This study has characterized the performance of a novel, second-generation, portable GC prototype, and has illustrated the performance tradeoffs associated with several key operating variables unique to an instrument with sensor array detection. Enhancements in design have led to significant improvements in sensitivity, resolution, flexibility, convenience, and overall performance relative to the previous prototype.[34]

The allowance for binary co-elutions afforded by the MPN-coated CR sensor array serves to distribute the analytical burden between the detection and separation modules and reduces the total analysis time; as shown, a 31-component mixture could be adequately separated in just seven minutes, and a complete sampling and analytical cycle could be completed in about 16 minutes. LODs for most compounds are in the sub-ppb range for a 1-L air sample, which are sufficiently low for applications in indoor- and ambient air quality monitoring, occupational exposure assessments, homeland security, and breath monitoring.

Difficulty was encountered with compounds having vapor pressures below about 0.4 torr, owing to low desorption efficiencies from the PCI and to adsorption on unheated surfaces in the system. In the worst cases, calibrations are decidedly nonlinear, which may preclude accurate quantification. Heating the interconnections upstream and downstream of the separation module should reduce the latter problem. Increasing the PCI desorption temperature should reduce the former problem, but it is likely that difficulty with such semi-volatile compounds will persist, and removing them from the sample stream with a pre-trap may be necessary.[30]

Where feasible, on-column focusing should be used as a means of reducing injection bandwidths for less volatile compounds.[36] As shown here, split-flow injection can also improve resolution. While the relative loss of sensitivity is larger than the relative gain in resolution, the low detection limits achievable with modest air-sample volumes makes the sensitivity tradeoff more tolerable. It should be kept in mind, however, that the split ratio employed here was quite low, and that higher split ratios should afford even greater improvements in resolution.

The influence of flow rate on responses (peak areas) from the CR sensor array is significant and noteworthy. Low flow rates afford higher sensitivity, but the sharp dependence of the peak area on the flow rate below 0.5 mL/min (measured at the outlet) argues for operating at higher flow rates where the dependence is much lower (and where chromatographic efficiency is also higher). The dependence of peak heights on flow rate, however, is much less than that of the peak areas and, since LODs are calculated on the basis of peak height, they will be less subject to variations from flow rate changes. Response patterns derived from the peak areas of the sensors in the array are also insensitive to flow rate.

Reductions in the vapor-MPN partition coefficients at elevated temperature lead to predictable reductions in sensitivity. For the less volatile compounds, this leads to a significant reduction in peak width and, therefore, increased resolution. Since such compounds yield unusually broad peaks at lower temperatures, and sensitivities are inherently high because of their large partition coefficients, it is worth considering operation of the sensor array at elevated temperature when targeting such less volatile compounds in an analysis.

The drifts in the baselines and in the sensitivities of the MPN-coated CR sensors observed during this study became significant after about two weeks of operation. The practical implication is the need for fairly frequent recalibration. Since this behavior is most likely due to movement of the nanoparticles within the film, we are exploring approaches to immobilization, including in situ cross-linking of the thiolate ligands, in an attempt to reduce this source of instability.

The versatility and analytical power embodied in this instrument exceed those of most other portable GCs by virtue of the integration of modules for preconcentration/injection, tunable separation, and sensor-array detection. All of these components are amenable to further miniaturization, and efforts to create micro-scale GC prototypes with similar features are underway.[15] The characterizations provided here have revealed several aspects of the performance of these components and their integration into a working system that should aid such efforts.

Acknowledgements

The prototype GC was constructed by a team at Microsensor Systems, Inc., Bowling Green, KY, led by Hank Wohltjen and Brent Busey, who provided continuing technical support throughout this project. The authors are indebted to these individuals for their hard work and dedication. The authors also wish to thank Professor Chia-Jung Lu for technical guidance and advice; Steve Parus for writing most of the LabVIEW code for data acquisition; Michael P. Rowe for MPN syntheses; and Sun Kim for technical support. Primary funding was provided by Grant No. R01-OH03692 from the National Institute for Occupational Safety and Health of the Centers for Disease Control and Prevention (NIOSH-CDCP). This work made use of Engineering Research Centers Shared Facilities supported by the National Science Foundation under Award Number EEC-0096866.

References

1 B. Cohen and C. S. McCammon, ed. *Air Sampling Instruments for Evaluation of Atmospheric Contaminants*, 9th edn, American Conference of Governmental Industrial Hygienists, Cincinnati, Ohio, 2001.
2 D. L. Miller, J. S. Woods, K. W. Grubaugh and L. M. Jordon, *Environmental Science & Technology*, 1980, **14**(1), 97–100.
3 N. J. Barker and R. C. Leveson, *American Laboratory*, 1980, **12**(12), 76.
4 Photovac, Inc. homepage, http://www.photovac.com (accessed Feb. 2008).
5 SRI Instruments homepage, http://www.srigc.com (accessed Feb. 2008).
6 Microsensor System Inc. homepage, http://microsensorsystems.com (accessed, March, 2008).
7 Varian, Inc. homepage, http://www.varianinc.com (accessed Feb. 2008).
8 Agilent Technologies homepage, http://www.home.agilent.com (accessed Feb. 2008).
9 Inficon homepage, http://www.inficon.com (accessed Feb. 2008).
10 Electronic Sensor Technology homepage, http://www.estcal.com (accessed Feb. 2008).
11 RVM Scientific Inc. homepage, http://www.rvmscientific.com (accessed Feb. 2008).
12 K. M. Sloan, R. V. Mustacich and B. A. Eckenrode, *Field Anal. Chem. Technol.*, 2001, **5**(6), 288–301.
13 SLS Micro Technology homepage, http://www.sls-microtechnology.de (accessed Feb. 2008).
14 Defiant Technologies homepage, http://www.defiant-tech.com (accessed Feb. 2008).
15 C. J. Lu, W. H. Steinecker, W. C. Tian, M. Agah, J. M. Potkay, M. C. Oborny, J. Nichols, H. Chan, J. Driscoll, R. D. Sacks, S. W. Pang, K. D. Wise and E. T. Zellers, *Lab Chip*, 2005, **5**, 1123–1131.
16 P. R. Lewis, R. P. Manginell, D. R. Adkins, R. J. Kottenstette, D. R. Wheeler, S. S. Sokolowski, D. E. Trudell, J. E. Byrnes, M. Okandan, J. M. Bauer, R. G. Manley and G. C. Frye-Mason, *IEEE Sens. J.*, 2006, **6**(3), 784–795.
17 E. T. Zellers, S. Reidy, R. A. Veeneman, R. Gordenker, W. H. Steinecker, G. R. Lambertus, H. Kim, J. A. Potkay, M. P. Rowe, Q. Zhong, C. Avery, H. K. L. Chan, R. D. Sacks, K. Najafi and K. D. Wise, "*An Integrated Micro-Analytical System for Complex Vapor Mixtures*," Proc. Transducers' 07, Lyon, FR, June 10–14, 2007, pp. 1491–1496.
18 C2V Company homepage, http://www.c2v.nl/(accessed Sept. 2008).
19 J. M. Sanchez and R. D. Sacks, *J. Sep. Sci.*, 2007, **30**(7), 1052–1060.
20 X. Liu and J. Pawliszyn, *J. Int. J. Environ. Anal. Chem.*, 2005, **85**(15), 1189–1200.
21 J. A. Dziuban, J. Mroz, M. Szczygielska, M. Malachowski, A. Gorecka-Drzazga, R. Walczak, W. Bula, D. Zalewski, L. Nieradko, J. Lysko, J. Koszur and P. Kowalski, *Sens. Actuators, A*, 2004, **115**, 318–330.
22 J. Ji, C. H. Deng, W. W. Shen and X. M. Zhang, *Talanta*, 2006, **69**(4), 894–899.
23 P. A. Smith, M. T. Sng, B. A. Eckenrode, S. Y. Leow, D. Koch, R. P. Erickson, C. R. Jackson Lepage and G. L. Hook, *J. Chromatogr. A*, 2005, **1067**, 285–294.
24 Griffin Analytical technologies homepage, http://www.griffinanalytical.com (accessed Feb. 2008).
25 R. P. Ericson, A. Tripathi, W. M. Maswadeh, A. P. Snyder and P. A. Smith, *Anal. Chim. Acta*, 2006, **556**(2), 455–461.
26 Femtoscan homepage, http://www.femtoscan.com (accessed Feb. 2008).
27 G. R. Lambertus, C. S. Fix, S. M. Reidy, R. A. Miller, D. Wheeler, E. Nazarov and R. D. Sacks, *Anal. Chem.*, 2005, **77**(23), 7563–7571.
28 C. Jia, S. Batterman and C. Godwin, *Atmos. Environ.*, 2008, **42**(9), 2083–2100.
29 S. A. Batterman, C. Y. Peng and J. Braun, *Atmospheric Environment*, 2002, **36**(39–40), 6015–6030.
30 Q. Zhong, R. A. Veeneman, W. H. Steinecker, C. Jia, S. A. Batterman and E. T. Zellers, *J. Environ. Monit.*, 2007, **9**, 440–448.
31 M. Phillips, *Anal. Biochem.*, 1997, **247**, 272–78.
32 M. Phillips, J. Herrera, S. Krishnan, M. Zain, J. Greenberg and R. N. Cataneo, *J. Chromatogr. B*, 1999, **729**, 75–88.
33 M. Y. Jia, J. Koziel and J. Pawliszyn, *Field Anal. Chem. Technol.*, 2000, **4**, 73–84.
34 C. J. Lu, J. J. Whiting, R. D. Sacks and E. T. Zellers, *Anal. Chem.*, 2003, **75**(6), 1400–1409.
35 C. J. Lu and E. T. Zellers, *Anal. Chem.*, 2001, **73**, 3449–3457.
36 C. J. Lu and E. T. Zellers, *Analyst*, 2002, **127**, 1061–1068.
37 C. J. Lu, C. Jin and E. T. Zellers, *J. Environ. Monit.*, 2006, **8**(2), 270–278.
38 Q. Y. Cai and E. T. Zellers, *Anal. Chem.*, 2002, **74**, 3533–3539.
39 J. J. Whiting and R. D. Sacks, *J. Sep. Sci.*, 2006, **29**(2), 218–227.
40 A. J. Grall and R. D. Sacks, *Anal. Chem.*, 1999, **71**(22), 5199–5205.
41 A. J. Grall, E. T. Zellers and R. D. Sacks, *Environ. Sci. Technol.*, 2001, **35**, 163–169.
42 W. H. Steinecker, M. P. Rowe and E. T. Zellers, *Anal. Chem.*, 2007, **79**, 4977–4986.
43 M. P. Rowe, K. E. Plass, K. Kim, C. Kurdak, E. T. Zellers and A. J. Matzger, *Chem. Mater.*, 2004, **16**, 3513–3517.
44 H. Wohltjen and A. W. Snow, *Anal. Chem.*, 1998, **70**, 2856–2859.
45 E. T. Zellers, S. A. Batterman, M. Han and S. J. Patrash, *Anal. Chem.*, 1995, **67**, 1092–1106.
46 J. Park, W. A. Groves and E. T. Zellers, *Anal. Chem.*, 1999, **71**, 3877–3886.
47 G. O. Nelson, *Gas Mixture: Preparation and Control*, Lewis, New York, 1992.
48 A. M. Kummer, A. Hielemann and H. Baltes, *Anal. Chem.*, 2004, **76**(9), 2470–2477.
49 S. M. Briglin and N. S. Lewis, *J. Phys. Chem. B*, 2003, **107**, 1103–11042.
50 J. F. Feller, D. Langevin and S. Marais, *Synthetic Metals*, 2004, **144**(1), 81–88.
51 W. Jennings, E. Mittlefehldt and P. Stremple, ed., *Analytical Gas Chromatography*, Academic Press, San Diego, CA, 2nd edn, 1997, pp. 145.
52 C. Jia, S. Batterman and S. Chernyak, *J. Environ. Monit.*, 2006, **8**(2), 1029–1042.
53 P. H. Howard and W. M. Meylan, *Handbook of Physical Properties of Organic Chemicals*, Lewis, New York, 1997.